Politecnico di Torino

Master of science program in ICT for Smart Societies LM-23
Collegio di Ingegneria Elettronica, delle Telecomunicazioni e Fisica (ETF)

Computationally Optimized 3D Stack-Of-Spirals Image Reconstruction

Supervisors:

- Prof. Danillo Demarchi (DET, Polito)
- Prof. Benedikt Poser (Maastricht University, Netherlands)

Candidate:

- Zoia Laraib s290062

ABSTRACT

Spiral readout trajectories have become popular in several applications of 2D and 3D MR imaging applications because of their ability to acquire more data in less time than their traditional Cartesian counterparts. 3D sampling is especially desirable for high-resolution imaging, which results in the combined burden of the (i) complexity inherent to non-Cartesian reconstruction, (ii) large data matrices for high resolution, and (iii) the need to process the entire 3D dataset in one go (instead of slice-by-slice as in 2D). The consequences are high computational cost and memory requirements during reconstruction, especially with parallel imaging and off-resonance correction. This research aims to improve the computational efficiency of the reconstruction methods while maintaining the accuracy of the resulting 3D images. Several challenges need to be addressed to improve the accuracy and efficiency of 3D imaging, such as incomplete k-space coverage, motion artifacts, noise, and field inhomogeneities. A four-step approach is proposed to optimize the 3D spiral reconstruction process for high-resolution single-shot under-sampled spirals and with correction for magnetic field inhomogeneities. Optimal k-space coverage and artifact minimization are critical for selecting an appropriate spiral trajectory.

Iterative reconstruction methods have been widely implemented for accurate and efficient image reconstruction, but optimization of these methods, especially 3D, can be time-consuming and computationally expensive. This work uses the high-level programming language Julia, which recently emerged as a powerful tool for implementing iterative reconstruction methods due to its speed and built-in support for parallel computing. By combining Julia with iterative reconstruction methods, we find that the efficiency and accuracy of MR image reconstruction can be greatly enhanced: Julia's multi-threading and distributed computing support can significantly reduce the reconstruction time for large datasets. At the same time, its built-in libraries for linear algebra and optimization can simplify the implementation of complex algorithms. This is exploited in computational optimization strategies and image quality in 3D imaging using spiral trajectories, focusing on reducing reconstruction time, minimizing the g-factor, and using pseudo-replica methods to analyze image variability. The optimizations proposed in this work are an important step towards achieving real-time high-quality 3D spiral reconstruction with a reduced computational burden. This will ultimately help applications in neuroimaging or clinical applications.

ACKNOWLEDGMENTS

This project is a tribute to my beloved parents, whose unwavering love, care, and support have impacted my life. Their steadfast dedication and constant encouragement have been instrumental in my success. Their prayers and generous assistance have been an integral part of the accomplishment of this project. Additionally, I would like to express my sincere appreciation to all our teachers who have taught us the importance of being responsible and professional in a practical environment. Their guidance has helped us develop the necessary technical skills and confidence to compete at an international level. Their commitment to our education has driven our achievements, and we will always be grateful for their unwavering support.

TABLE OF CONTENTS

LIST OF ILLUSTRATIONS

LIST OF TABLES

LIST OF GLOSSARIES OF ACRONYMS

MRI - Magnetic Resonance Imaging

MR - Magnetic Resonance

AP - Artifact Power

AF - Acceleration Factor

SNR - Signal-to-Noise Ratio

PE - Phase Encoding

FE - Frequency Encoding

CT - Computed Tomography

PET - Positron Emission Tomography

FFT - Fast Fourier Transform

GRAPPA - Generalized Auto Calibrating Partially Parallel Acquisitions

ACS - Auto Calibration Signals

FOV - Field-of-view

pMRI - parallel Magnetic Resonance Imaging

SENSE - Sensitivity Encoding

SOSP - Stack of Spirals

CGNR - Conjugate Gradient Normal Residual

ADMM - Alternating Direction Multiple Multipliers

VDSS – Variable Density Stack of Spirals

1 CHAPTER: INTRODUCTION

This chapter introduces Magnetic Resonance Imaging (MRI) and its advantages over other medical imaging techniques. The use of stack-of-spirals acquisition methods is discussed to reduce scan time and increase spatial resolution, but it also presents challenges. The thesis proposes an approach to optimize the reconstruction of high-resolution, single-shot, under-sampled spirals for 3D imaging while correcting for magnetic field inhomogeneities, to improve MR image reconstruction efficiency and accuracy.

Magnetic Resonance Imaging (MRI) is a non-invasive medical imaging technique that uses a powerful magnetic field and radio waves to generate detailed images of the body's internal structures. MRI was first developed in the 1970s and has become an essential tool for diagnosing various medical conditions [1]. It is especially useful in imaging soft tissues such as the brain, spinal cord, and organs.

MRI uses a strong magnetic field to align the hydrogen atoms in the body's tissues. Radio waves are then used to excite these atoms, causing them to emit signals that the MRI machine can detect. A computer processes the signals to generate detailed images of the body's internal structures. Unlike X-rays, which use ionizing radiation, MRI does not expose patients to harmful radiation, making it a safe and non-invasive option for medical imaging.

MRI has several advantages over other medical imaging techniques. One of the main advantages is its ability to provide detailed images of soft tissues such as the brain, spinal cord, and organs. This is particularly important in diagnosing and treating neurological conditions, cancer, and heart disease. MRI is also non-invasive and does not use ionizing radiation, making it safer than other imaging techniques such as X-rays and CT scans.

MRI is also very versatile and can be used to image almost any part of the body. It can be used to detect abnormalities in the brain, spine, joints, and organs and to guide surgical procedures. In addition, MRI can provide detailed information about the function of the brain and other organs, which is important in diagnosing and treating many medical conditions. Finally, MRI can also be used to monitor treatment progress, making it a valuable tool for assessing the effectiveness of therapies.

MRI has some disadvantages, including high cost and long acquisition. Moreover, the examination process can be uncomfortable for patients, as they have to remain immobile for long periods while lying inside the scanner's bore. Even minor movements during the scan can result in image motion artifacts, affecting the diagnostic quality. Patients with certain implanted devices, such as pacemakers, cannot undergo MRI due to safety concerns. Despite these limitations, MRI remains an essential tool in modern medical imaging because it provides high-resolution images of the internal organs, soft tissues, and bones without ionizing radiation.

Ongoing research is focused on developing new technologies and techniques to improve MRI speed, comfort, and diagnostic accuracy while minimizing its limitations.

Conventionally, In MR imaging, k-space is sampled along a grid of lines, resulting in a rectangular shape. This method has been the standard for many years and is widely used in clinical practice. However, it has several limitations, such as a low signal-to-noise ratio and long acquisition times. There has been growing interest in using spiral acquisition techniques for high spatial resolution and faster scan time.

The stack-of-spirals acquisition method collects k-space data by acquiring a series of 2D spiral trajectories at different angles and then stacking them to form a 3D volume. This method has several advantages, including a higher signal-to-noise ratio, shorter acquisition times, and improved spatial resolution.

One of the main advantages of the stack-of-spirals method is that it allows for more efficient coverage of k-space, which contains raw MR data, which leads to faster acquisition times. Additionally, using spirals provides data acquisition along multiple orientations, improving image quality and reducing artifacts. Another advantage is that the spirals can be tailored to specific applications, such as imaging different organs or tissues.

Despite these advantages, there are some challenges associated with using stack-of-spirals imaging. One of the main challenges is that off-resonance effects can be more severe in 3D spiral acquisitions due to the longer readout times. Additionally, the reconstruction of the 3D volume from the stack of 2D images can be computationally intensive.

This study aims to propose approaches to optimize the reconstruction process of high-resolution, single-shot, under-sampled spirals for 3D imaging while correcting for magnetic field inhomogeneities. The proposed system aims to minimize artifacts and optimize k-space coverage to enhance the efficiency and accuracy of MR image reconstruction.

To achieve this, the study combines Julia, a high-level programming language with built-in support for parallel computing, with iterative reconstruction methods [5]. By leveraging Julia's multi-threading and distributed computing support, the proposed approach aims to reduce the reconstruction time for large datasets while simplifying the implementation of complex algorithms.

2 CHAPTER: THEORETICAL FRAMEWORK FOR MRI AND IMAGE RECONSTRUCTION

This chapter provides a comprehensive background to the theoretical concepts and principles essential to understanding the research presented in this thesis. The chapter covers various topics, including the basic principles of magnetic resonance imaging, image acquisition, k-space, Fourier transformation, and the multiple techniques used for image reconstruction, such as iterative and parallel imaging. Additionally, the chapter delves into the theory behind spiral trajectories and gridding approaches used for non-cartesian techniques and their advantages over conventional Cartesian imaging techniques. This chapter aims to provide readers with a strong foundation in the theoretical aspects of MRI and image reconstruction. It serves as a crucial primer for the subsequent chapters of this thesis.

Parallel MRI (pMRI) is a widely used imaging technique that can significantly reduce the scanning time, accelerate data acquisition, and improve spatial resolution and image quality [19]. pMRI uses an array of independent receiver coils with different sensitivity profiles for parallel data acquisition. A special algorithm is used to reconstruct unaliased images from the under-sampled data. The advantages of pMRI have made it a valuable tool in clinical diagnostics.

2.1 MR DATA ACQUISITION AND IMAGE FORMATION

MR data acquisition and image formation involve a complex interplay of hardware and software components. The basic principle of MRI is that when the body is placed in a strong magnetic field, the protons in the water molecules align themselves with the magnetic field. Radiofrequency (RF) pulses are applied to the body, causing the protons to flip out of alignment with the magnetic field. When the RF pulse is turned off, the protons release energy and return to their original alignment, emitting a radiofrequency signal that can be detected by the MRI scanner [4].

The MRI scanner detects the signals emitted by the protons and uses them to create images of the body. MR data acquisition involves collecting a series of signals to construct an image. The process of acquiring MR data involves several steps, including encoding the spatial information of the signal, collecting the signal, and processing the data to create an image. After data acquisition, an appropriate image reconstruction method is applied to reconstruct the fully sampled image from the under-sampled image data. The frequency-domain signal can then be used to construct an image.

The digital data is stored in a two-dimensional grid called k-space, which contains information about the spatial frequency of the protons. Reconstructing an image from k-space data involves performing an inverse Fourier transform, which converts the frequency information back into the spatial domain. Filtering is applied to the image to remove noise and improve image quality. MR data acquisition and image formation are complex processes that require careful calibration and optimization.

2.1.1 k-SPACE

During MRI data acquisition, k-space is the raw data space that stores the digitized MR signal. It captures a vast amount of information from real space, with the size of the k-space being determined by the frequency encoding and phase encoding steps. The k-space contains all the information required to construct an image, and the contrast and signal-to-noise information of an image are stored at the center of the k-space.

The data located at the center of the k-space corresponds to low spatial frequencies, while the data at the periphery represent high spatial frequencies. It is crucial to fulfilling the Nyquist criteria while sampling to obtain an unaliased and artifact-free image. The Fourier Transform links the image domain and k-space domain.

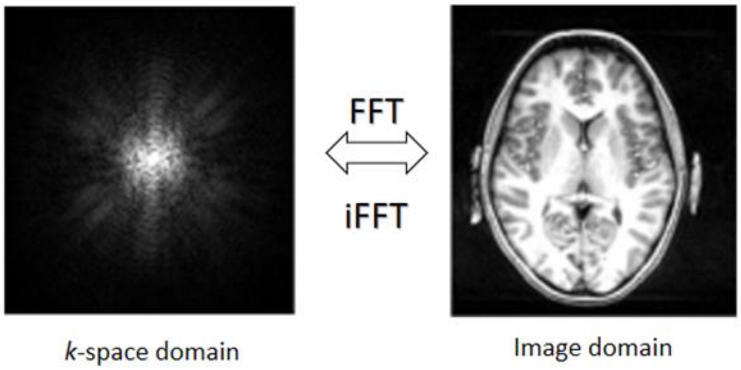

Figure 2.1 Relation between k-space & image domain

2.1.2 k – SPACE TRAJECTORIES

Data is acquired in k-space in various ways. The most common method is 2D Cartesian acquisitions, where images are obtained by reading outlines in a grid pattern. However, this method can be time-consuming and prone to motion artifacts. Alternative acquisition trajectories, such as spiral trajectories, have been developed to overcome these limitations.

Spiral trajectories are a non-Cartesian acquisition method where k-space data is collected along spiral paths rather than grid patterns. This allows for faster acquisition times, reduced motion artifacts, and increased signal-to-noise ratio (SNR). However, spiral imaging can be challenging to implement due to off-resonance effects and computational costs. Despite the challenges, the advantages of spiral images have made them popular in 3D imaging applications, such as neuroimaging and cardiac imaging. Spiral imaging can acquire more data in less time, reducing the scan time and potentially improving patient comfort.

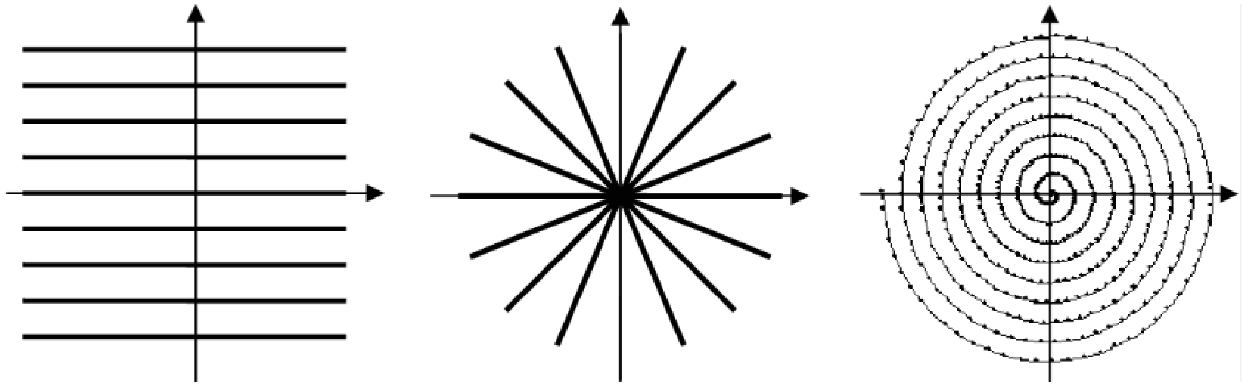

Figure 2.2 Types of Trajectories left to right: Cartesian, radial, spiral.

Radial trajectories are another commonly used method for acquiring MRI data. In radial trajectories, the k-space is sampled by acquiring data in a series of radial lines emanating from the center of the k-space. This sampling method offers several advantages over traditional Cartesian sampling. Firstly, radial trajectories are inherently more robust to off-resonance effects and motion artifacts, as they sample the k-space in a more distributed manner. Additionally, radial trajectories can provide more efficient coverage of the k-space than Cartesian trajectories, resulting in shorter scan times. However, a disadvantage of radial trajectories is that they typically require more sophisticated reconstruction algorithms, such as iterative or compressed sensing techniques, to generate high-quality images from the acquired data.

2.2 PARALLEL IMAGING

Parallel Magnetic Resonance Imaging (pMRI) is a technique used in medical imaging that allows for faster acquisition of images by utilizing multiple receiver coils to collect data simultaneously.

Two common techniques used in pMRI are GRAPPA (GeneRalized Autocalibrating Partial Parallel Acquisition) and SENSE (SENSitivity Encoding) [2]. GRAPPA is a method that uses the acquired data from neighboring coils to estimate the missing data in the center of the k-space, which can then be used to reconstruct the image [3]. SENSE, on the other hand, uses information from all coils to simultaneously acquire data from different regions of k-space, allowing for even faster acquisition times. Both techniques have been shown to be effective in reducing scan times while maintaining image quality in pMRI.

2.2.1 SPIRAL IMAGING

In 3D MRI, we use Stack-of-spiral, which employs multiple 2D spiral acquisitions performed in the axial plane with varying slice thicknesses and interleaved to form a 3D volume. The acquisition time of each 2D spiral acquisition is relatively short, making the technique robust to motion artifacts and allowing for high temporal resolution.

The spiral arms cover a larger k-space than a conventional Cartesian acquisition, enabling higher in-plane resolution. Additionally, using non-Cartesian trajectories like spirals allows for flexibility in sampling density, which can be optimized for specific applications.

Using a stack of spirals in MRI has numerous advantages over conventional imaging techniques. One of the key benefits is faster data acquisition, which leads to shorter scan times for patients. Compared to conventional methods, spiral trajectories can lead to shorter patient scan times, making it a valuable tool in clinical settings. This fast acquisition also allows for the acquisition of high temporal resolution data, making it particularly useful in functional MRI (fMRI) studies.

In functional MRI (fMRI) studies, spiral imaging has become increasingly popular due to its ability to provide high temporal resolution and whole-brain coverage, enabling researchers to capture rapid changes in brain activity across multiple regions simultaneously. Additionally, spiral imaging can minimize the effects of physiological noise and motion artifacts, leading to improved signal-to-noise ratios and more accurate functional connectivity measurements. These advantages make spiral imaging a valuable tool in fMRI research for investigating the neural underpinnings of various cognitive and behavioral processes.

2.2.2 LIMITATIONS OF USING A STACK OF SPIRALS

The off-resonance effect becomes more prominent as the length of the spiral arm increases, leading to image blurring or distortion. Field inhomogeneities refer to variations in the magnetic field strength across the imaging volume of an MRI scanner. Various factors, such as magnetic susceptibility differences between tissues or the presence of metallic objects, can cause these variations. Field inhomogeneities can cause image artifacts and distortions, reducing image quality and accuracy.

The reconstruction process for a 3D stack of spirals can be computationally intensive and time-consuming, especially when dealing with large datasets. Spiral imaging employs the use of gridding operation, which involves mapping the non-uniformly sampled k-space data onto a Cartesian grid, allowing fast Fourier transforms to reconstruct the image. However, this gridding process can be computationally expensive and time-consuming, especially for high-resolution images in 3D MRI.

These limitations can be a concern when dealing with certain types of data, such as those with low SNR or requiring a high spatial resolution. To overcome these limitations, it is important to carefully optimize the parameters of the spiral trajectory and image reconstruction methods.

This thesis mainly focuses on optimizing the k-space acquisition process while reducing the computational intensity. This is achieved by optimizing the reconstruction methods by selecting the best parameters, which serve as the bottleneck in image reconstruction. By doing so, the efficiency and accuracy of image reconstruction can be improved, enabling faster and more reliable patient diagnoses.

2.3 FIELD INHOMOGENEITY

The images produced by MRI can be affected by geometric distortions in the spatial domain, which are caused by field inhomogeneities. Field inhomogeneities refer to the variation in the strength of the magnetic field across the region of interest, which leads to distortions in the image.

Several factors contribute to field inhomogeneity in MRI. The main element is the main field inhomogeneity, which can be caused by variations in the magnetic field strength across the imaging region. This can be due to imperfections in the magnetic field produced by the MRI scanner or variations in the magnetic susceptibility of the tissues being imaged.

Magnetic susceptibility refers to the ability of a material to become magnetized in the presence of a magnetic field. The presence of materials with high magnetic susceptibilities, such as iron or other metals, can cause field inhomogeneities in the surrounding tissues. Additionally, chemical shifts, which occur due to differences in the resonant frequencies of protons in different molecules, can also contribute to field inhomogeneity.

Another factor that can contribute to field inhomogeneity is the presence of metal implants in the body. Metal implants can produce strong magnetic fields that can distort the magnetic field in the surrounding tissues, leading to image distortions.

2.3.1 FIELD INHOMOGENEITY CORRECTION METHOD

To address these distortions, various correction methods can be employed in MRI. One common approach is to use post-processing algorithms to correct geometric distortions caused by field inhomogeneity. These correction techniques can help to improve the quality of MRI images and reduce the impact of field inhomogeneities on the final image. An example of a distorted MRI image caused by field inhomogeneities is shown in Figure 2.3.

One commonly used method is deconvolution, which involves the removal of the convolution effect caused by the off-resonance effects on the image. This method can be computationally intensive, and the correction accuracy may be limited by the assumptions made in the deconvolution process.

Another method is autofocusing, which involves iterative phase estimation to correct the off-resonance effects. This approach involves iterative estimation of the phase error, which is then used to correct the image. Autofocusing can be computationally efficient but may not be suitable for all imaging scenarios.

Model-based image reconstruction is another approach that can be used to correct off-resonance effects. This method involves forward modeling the image acquisition process, including the off-resonance effects, and then estimating the image using an optimization algorithm. Model-based image reconstruction can be computationally intensive but can provide accurate correction for off-resonance effects.

Efficient approximation methods can also be used to correct off-resonance effects. These methods involve approximating the off-resonance effects using simpler models, which can then be corrected using simpler algorithms. While these methods may not provide the same level of accuracy as the other methods, they can be computationally efficient and suitable for real-time imaging applications.[14]

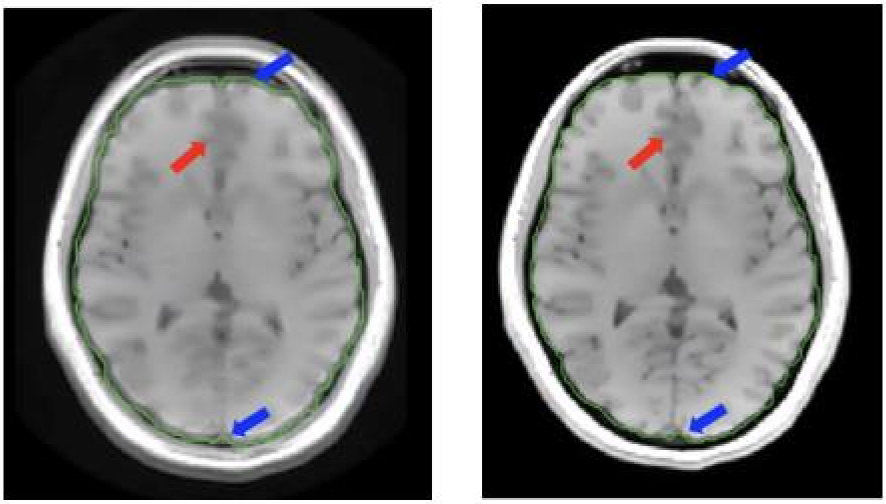

Figure 2.3 An example of off-resonance effects in spiral imaging. The image on the left shows a distorted image due to the off-resonance impacts, while the image on the right shows the corrected image after applying one of the correction methods.

2.4 NON-UNIFORM FAST FOURIER TRANSFORM

In spiral imaging, the k-space data is typically reconstructed onto a Cartesian grid to enable common Fast Fourier Transform algorithms. However, this gridding approach can induce computational costs and potential errors. As an alternative, Non-uniform Fast Fourier Transform (NUFFT) methods can be used to directly transform non-uniformly sampled data to a Cartesian grid without gridding. NUFFT methods have been shown to reduce computational time and improve accuracy in spiral imaging compared to traditional gridding methods. Thus, NUFFT has become a popular approach for image reconstruction in spiral imaging, particularly in fMRI studies where fast acquisitions and high resolution are critical for capturing dynamic brain activity.

The NUFFT algorithm involves several steps, including calculating the frequency-domain representation of the non-uniform data, followed by a scaling and convolution operation to generate the final grid of Fourier coefficients. The computational cost of the NUFFT algorithm can be quite high, particularly for large data sets, making it necessary to employ optimization techniques to reduce the computational burden.

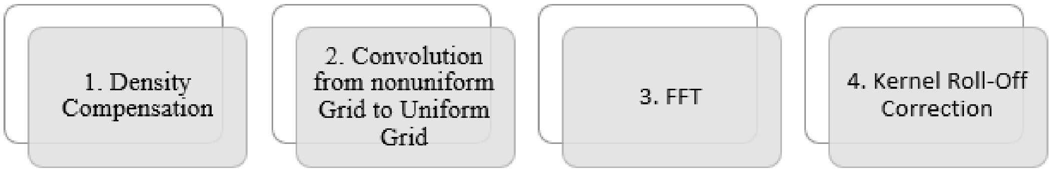

Figure 2.4 Steps of NUFFT

The first step in this process is Density Compensation, which involves multiplying the raw k-space data by a density compensation function to correct for the non-uniform sampling density.

Next, Convolution from a non-uniform Grid to Uniform Grid is performed by convolving the density-compensated k-space data with a kernel function. This step is necessary to interpolate the data onto a uniform Cartesian grid.

Once the data has been interpolated onto a uniform grid, Fast Fourier Transform (FFT) is applied to the k-space data to obtain the image data. However, due to the non-uniform sampling, the k-space data requires a Kernel Roll-Off Correction, a high-pass filtering step to correct the roll-off in the image resolution at high spatial frequencies.[15]

Figure 2.4 shows the steps in the image reconstruction process, including Density Compensation, Convolution from non-uniform Grid to Uniform Grid, FFT, and Kernel Roll-Off Correction.

2.5 ITERATIVE RECONSTRUCTION METHOD

This section introduces and compares two methods, CGNR and ADMM, for reconstructing MRI images from under-sampled data with different regularizers. The study presents the theoretical framework and the experimental results of each method.

2.5.1 CONJUGATE GRADIENT SENSE RECONSTRUCTION

CG SENSE (Conjugate Gradient SENSE) is a fast iterative reconstruction algorithm that is commonly used in magnetic resonance imaging (MRI)[17]. It uses sensitivity map estimations to improve image quality and reduce image artifacts. The algorithm is particularly efficient for non-cartesian acquisition trajectories, commonly used in spiral imaging.

CG SENSE works by iteratively solving linear equations using a conjugate gradient method. These equations incorporate the sensitivity maps of the MRI coils, which describe the spatial variation in sensitivity of the coils across the imaging region. Using these sensitivity maps, CG SENSE can partially compensate for off-resonance due to gridding/regridding, which can cause image distortions in non-cartesian acquisitions.

The main advantage of CG SENSE is its computational efficiency, which allows for rapid image reconstruction from large datasets. Additionally, the algorithm is highly adaptable and can be modified to incorporate various acquisition parameters, such as field strength and coil configuration, to optimize image quality. However, CG SENSE does have some limitations, including its sensitivity to noise and the accuracy of the sensitivity maps used.[17]

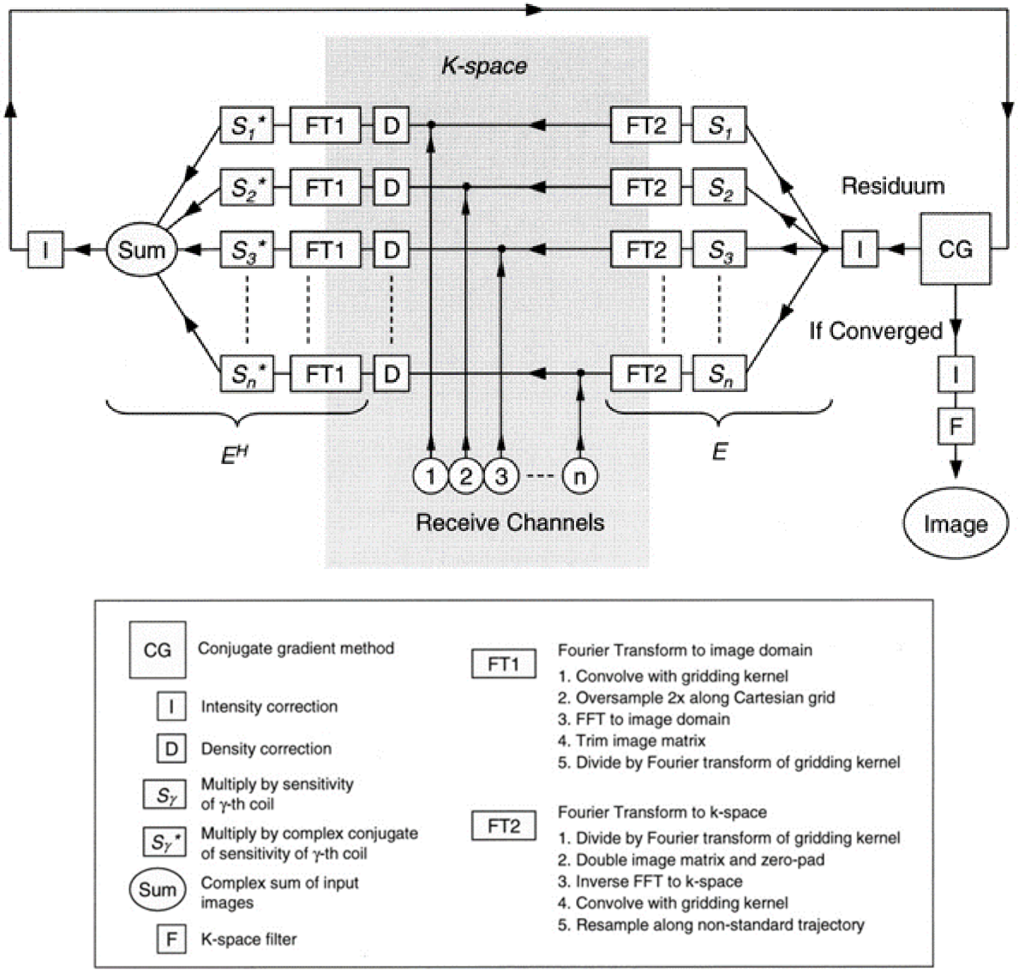

Figure 2.5 CG-SENSE Algorithm

2.5.2 ALTERNATING DIRECTION METHODS OF MULTIPLIERS

ADMM (Alternating Direction Method of Multipliers) is a popular algorithm for solving optimization problems in image reconstruction. In MRI, ADMM reconstruction involves solving an optimization problem to obtain a high-quality image from the under-sampled k-space data acquired using a spiral trajectory.[18] The ADMM algorithm splits the original optimization problem into smaller sub-problems, which can be solved iteratively using alternating minimization.

In the case of spiral MRI, the ADMM reconstruction algorithm involves solving for the image and the k-space data separately. This is done by iteratively solving two sub-problems: one for the image and one for the k-space data. The image sub-problem involves minimizing the L1 norm of the image subject to the constraint that the image matches the acquired k-space data.

The ADMM algorithm has been shown to be effective for spiral MRI reconstruction because it can handle the non-linear and non-convex optimization problem that arises due to the under-sampled k-space data. [18]. It also allows for incorporating additional constraints, such as total variation regularization, for improving the quality of the reconstructed image. The ADMM algorithm is computationally efficient, making it suitable for real-time image reconstruction in clinical settings.

In Julia Programming Language, ADMM can be implemented using the RegularizedLeastSquares.jl. The ADMM method for regularized least squares can be formulated as follows:

$$minimize \frac{1}{2}||Ax - b||_2^2 + \lambda * ||x||_1$$

where A is the measurement matrix, b is the measured data, x is the unknown image, λ is the regularization parameter, and $||.||_1$ is the L1 norm.

The ADMM method splits the original problem into two sub-problems: one for x and one for z, where z is an auxiliary variable that enforces the sparsity constraint. The two sub-problems are:

$$x^{k+1} := \frac{argmin_x 1}{2} \left|\left|Ax - b\right|\right|_2^2 + \frac{\rho}{2} \left|\left|x - z^k + u^k\right|\right|_2^2$$

$$z^{k+1} := \frac{argmin_{z\lambda}}{rho} \left|\left|z\right|\right|_1 + \frac{1}{2} \left|\left|x^{k+1} - z + u^k\right|\right|_2^2$$

Where ρ is a penalty parameter, and u is a dual variable that enforces the consistency between x and z. The dual variable is updated as follows:

$$u^{k+1} := u^k + x^{k+1} - z^{k+1}$$

The algorithm iterates until convergence, which can be checked using some stopping criteria based on the primal and dual residuals.

The following pseudo-code summarizes the ADMM method for regularized least squares:

```
$Given\ A, b, \lambda, \rho$
$Initialize\ x, z, u$
$repeat$
 $(\ \#\ update\ x\ by\ solving\ a\ least\ squares\ problem)$
  $x := (A^T A + \rho I)^{-1}(A^T b + \rho (z - u))$
 $(\ \#\ update\ z\ by\ applying\ soft - thresholding)$
  $z := \frac{S_\lambda}{\rho} \rho (x + u)$
 $(\ \#\ update\ u\ by\ adding\ the\ difference\ between\ x\ and\ z)$
  $u := u + x - z$
until convergence
```

where S_τ is the soft-thresholding operator defined as:

$$S_{\tau(v)_i} = sign(v_i) * \max(|v_i| - \tau, 0)$$

for each element i of the vector v.

The penalty parameter ρ controls the trade-off between the primal and dual feasibility of the ADMM algorithm. A small value of ρ means that the algorithm will focus more on satisfying the primal constraints, while a large value of ρ means that the algorithm will focus more on satisfying the dual constraints. The optimal value of ρ depends on the problem structure and the desired accuracy. Primal residual is the difference between the primal variables x and z in ADMM, which should be zero at optimality. Similarly, Dual residual are the difference between two consecutive values of the dual variable y in ADMM, which should be zero at optimality.

3 CHAPTER: IMPLEMENTATION

Implementing image reconstruction simulations is a crucial aspect of MRI technology development. This chapter explores the implementation of image reconstruction simulations using MATLAB for simulating pulse sequences, data, and trajectories. It also implements image reconstruction in Julia language and compares the results by tuning parameters. Different reconstruction methods, such as conjugate gradient and ADMM, are explored to identify the optimal approach for a specific application. The chapter provides a comprehensive overview of the implementation of image reconstruction simulations, covering both MATLAB and Julia programming languages. It aims to optimize the image reconstruction process and obtain high-quality images from acquired MRI data.

3.1 MATLAB

MATLAB is a powerful numerical computing environment widely used for various scientific and engineering applications. It provides a high-level programming language and interactive development environment, enabling users to perform complex numerical computations and visualizations easily. MATLAB has many built-in functions and toolboxes that facilitate various applications, including image processing, signal processing, and control system design.

MATLAB is extensively used in image processing for various tasks such as image enhancement, image segmentation, and image restoration. It provides a rich set of image-processing functions and toolboxes that enable users to perform multiple operations on digital images. For instance, MATLAB Image Processing Toolbox includes functions for filtering, morphology, feature extraction, and object detection, which can be used to manipulate and analyze images. Furthermore, MATLAB provides a graphical user interface (GUI) for interactive image processing, which allows users to explore and edit images visually. Overall, MATLAB is an essential tool for image processing, as it provides a convenient platform for performing advanced image analysis and manipulation tasks.

Pulseq is an open-source software package for designing and simulating magnetic resonance imaging (MRI) pulse sequences. It is a versatile tool that allows users to create customized pulse sequences for various imaging applications. Pulseq supports different pulse types and enables users to define arbitrary waveform shapes and timings. Moreover, it provides a simple and intuitive interface for designing pulse sequences and simulating their effects on the magnetization of the imaged object. Pulseq is intended to be compatible with various MRI scanner platforms, and its output can be directly exported to the scanner for execution. The software is continuously updated and maintained by a community of researchers, making it a reliable and up-to-date tool for MRI pulse sequence design and simulation. Pulseq is a valuable resource for researchers and engineers working in the field of MRI, as it provides a flexible and customizable platform for pulse sequence design and simulation.

3.2 JULIA PROGRAMMING LANGUAGE

Julia is a high-performance, dynamic programming language designed specifically for numerical and scientific computing but is also suitable for general-purpose programming [5]. The language was first introduced in 2012 by a team of researchers led by Alan Edelman, Jeff Bezanson, Stefan Karpinski, and Viral Shah. The main goal of the Julia programming language was to address the shortcomings of existing scientific programming languages, such as slow performance, limited parallelism, and lack of usability. Julia is designed to be easy to use, high-performance, and provide an interactive and exploratory environment for scientific computing. One of the key features of Julia is its speed, which is comparable to low-level programming languages like C and Fortran. Julia achieves this speed using a Just-In-Time (JIT) compiler and a type inference system that can optimize the code at runtime.

Since its introduction, Julia has gained significant popularity in the scientific computing community, and it has been adopted by many researchers, companies, and institutions for various applications. Julia's performance, ease of use, and interactive environment make it an attractive choice for scientific computing tasks that require high-performance computing, such as image processing, machine learning, and data analysis. Moreover, the language's growing package ecosystem provides tools and libraries for various scientific computing tasks.

Julia has several advantages, including speed, interactivity, and parallelism, compared to other scientific programming languages, such as MATLAB, Python, and R. Moreover, Julia's syntax is designed to be similar to mathematical notation, making it easy for scientists and engineers to translate their mathematical ideas into code. These features make Julia an attractive option for MRI reconstruction tasks, which often require high-performance computing and involve complex mathematical operations. The MRIReco.jl package is an example of the use of Julia for MRI reconstruction and demonstrates the potential of the language for this task[9].

3.3 MRIReco.jl

MRIReco.jl is a software package for image reconstruction in magnetic resonance imaging (MRI). It is a flexible and customizable tool that provides a comprehensive set of functionalities for image reconstruction. MRIReco.jl is written in Julia programming language, which enables it to leverage Julia's high-performance capabilities and distributed computing support.

The combination of high-level and low-level languages is widely used in the field of MRI, and two popular software packages that follow this approach are Gadgetron [6] and BART [7]. These packages have various features and are primarily written in C/C++, with bindings available for high-level languages. However, SigPy, [7] takes a different approach, which is a high-level MRI package written entirely in Python. This design choice allows for quick experimentation and prototyping of different MRI reconstruction algorithms.

In contrast to SigPy, MRIReco.jl [9]is a package that is written in Julia, a high-level programming language with a syntax similar to that of MATLAB or Python. The package is designed to provide a flexible and user-friendly platform for MRI image reconstruction.

MRIReco.jl provides a variety of image reconstruction methods, including iterative, compressed sensing, and deep learning-based approaches. It also supports reconstruction algorithms and regularization techniques, such as total variation and wavelet-based methods. MRIReco. jl's flexibility and versatility make it suitable for a wide range of applications, from clinical diagnosis to scientific research.

One of the key advantages of MRIReco.jl is its compatibility with different MRI scanner platforms. It supports various data formats and acquisition protocols, which enable users to work with data from different scanners and acquisition sequences. Moreover, the modular architecture allows for easy integration with other imaging tools and software packages.

MRIReco.jl is continuously updated and maintained by a community of researchers and developers, making it a reliable and up-to-date tool for MRI image reconstruction. Its open-source nature also enables users to contribute to its development and customization.

MRIReco.jl is a powerful and flexible software package for MRI image reconstruction. Its compatibility with different MRI scanner platforms, support for various reconstruction methods and algorithms, and modular architecture make it a valuable tool for researchers and clinicians working in MRI.

In this study, MRIReco.jl is used to compare different image reconstruction methods and optimization strategies for MRI data. [9]

4 CHAPTER: EXPERIMENTS & RESULTS

This section presents experiments to investigate the 3D reconstructions using CGNR and ADMM methods.

The CGNR method is a conjugate gradient algorithm that solves the normal equations of the least squares problem. It solves the inverse problem of reconstructing an image from the measured data, subject to some regularization term. The regularization term enforces some prior knowledge or constraints on the image, such as smoothness, sparsity, or positivity.

Tikhonov regularization is a technique that adds a penalty term to the loss function of a machine learning model, which is proportional to the sum of the squares of the model's weights. This penalty term reduces the complexity of the model by shrinking the weights towards zero, but not exactly zero. This helps to prevent overfitting and improve generalization.

In MRI reconstruction, Tikhonov regularization can be applied to the CGNR method, a conjugate gradient method for solving normal equations arising from linear least squares problems. The CGNR method iteratively updates the solution vector until it converges to the exact solution or the desired accuracy.

We want to optimize the reconstruction by finding the convergence of solutions for different values of the regularization parameter λ. To do this, we use the L-curve criterion, a graphical tool for choosing an optimal λ. The L-curve plots the residual norm (the error between the observed and predicted data) versus the solution norm (the magnitude of the solution vector) for different λ values. The optimal λ is usually located at the corner of the L-curve, where there is a good balance between data fit and solution smoothness.

Plotting the residual norm versus the number of iterations for a few λ values can lead to comparing their convergence rates and stability. Smaller λ values will require more iterations to converge but will produce more accurate solutions. Larger λ values will converge faster but produce smoother and less accurate solutions.

In this study, we use two types of L-curve plots to assess the performance of Tikhonov regularization in CGNR method for MRI reconstruction:

Residual norm versus different regularization values for the same dataset. This plot shows how different λ values affect a given dataset's data fit and solution smoothness. We expect an L-shaped curve with a clear corner point indicating an optimal λ.

Residual norm versus iterations for a few regularization values. This plot shows how different λ values affect the convergence rate and stability of the CGNR method. We expect to see those smaller values of λ result in lower residual norms but require more iterations to converge. Larger values of λ result in higher residual norms but converge faster.

4.1 CGNR METHOD

Table 4.1 shows the time taken for the CGNR method to converge on the value of λ, which is the regularization parameter that controls the trade-off between data fit and solution smoothness. This table suggests that there is an optimal range of λ values that minimize the time taken for convergence while avoiding overfitting or underfitting.

Table 4.1 Reconstruction time of 3D Phantom with different regularization

Regularization parameter	**Time (s)**
3e-1	1010.29
1e-1	966.47
3e-2	937.08
1e-2	964.12
3e-3	945.49
1e-3	939.45
1e-4	947.58

The above table indicates that the time taken for convergence decreases as λ decreases from 3e-1 to 3e-2, implying that smaller λ values result in faster convergence. This is because smaller λ values allow more flexibility in the solution vector, which can better fit the data and reduce the residual norm. However, this trend reverses when λ decreases further from 3e-2 to 1e-4, which implies that too small values of λ result in slower convergence. This is because too small values of λ lead to overfitting, which increases the complexity and instability of the solution vector.

Above table also shows that the minimum time taken for convergence occurs when λ is around 1e-3, which suggests this is an optimal λ value for this problem. This λ value provides a good balance between data fit and solution smoothness, resulting in a stable and accurate solution vector. This value of λ also corresponds to the corner point of the L-curve plot, which confirms its optimality.

Therefore, based on the table, we can conclude that Tikhonov regularization with the CGNR method can effectively solve ill-conditioned linear systems of equations with a suitable choice of λ. The optimal value of λ can be determined by using the L-curve criterion or by minimizing the time taken for convergence.

The convergence plots in Figures 4.1 & 4.2 show the residual norm versus the number of iterations for λ values of 3e-1 and 3e-2 for the in vivo data. The residual norm measures how well the solution satisfies the normal equations. The smaller the residual norm, the more accurate the solution.

The plots indicate that both λ values result in similar residual norms after 10 iterations, which suggests that the solution has converged to the desired accuracy. The plots also show that the convergence curves are smooth and stable, which implies that the CGNR method with Tikhonov regularization is robust and reliable.

The plots also reveal some differences between the two λ values. The plot for λ = 3e-1 shows a higher initial residual norm than the plot for λ = 3e-2, which implies that λ = 3e-1 fits the data worse than λ = 3e-2. However, the plot for λ = 3e-1 also shows a faster decrease in the residual norm than the plot for λ = 3e-2, which implies that λ = 3e-1 converges faster than λ = 3e-2. The plot for λ = 3e-2 shows a lower initial residual norm and a more gradual decrease in the residual norm, implying that λ = 3e-2 fits the data better and leads to a smoother solution.

Therefore, based on the convergence plots, we can conclude that Tikhonov regularization with the CGNR method can effectively solve ill-conditioned linear systems of equations with a suitable choice of λ. The optimal value of λ can be determined by using the L-curve criterion or by minimizing the time taken for convergence. For this problem, λ = 3e-2 seems to be a better choice than λ = 3e-1, as it provides a more accurate and smooth solution.

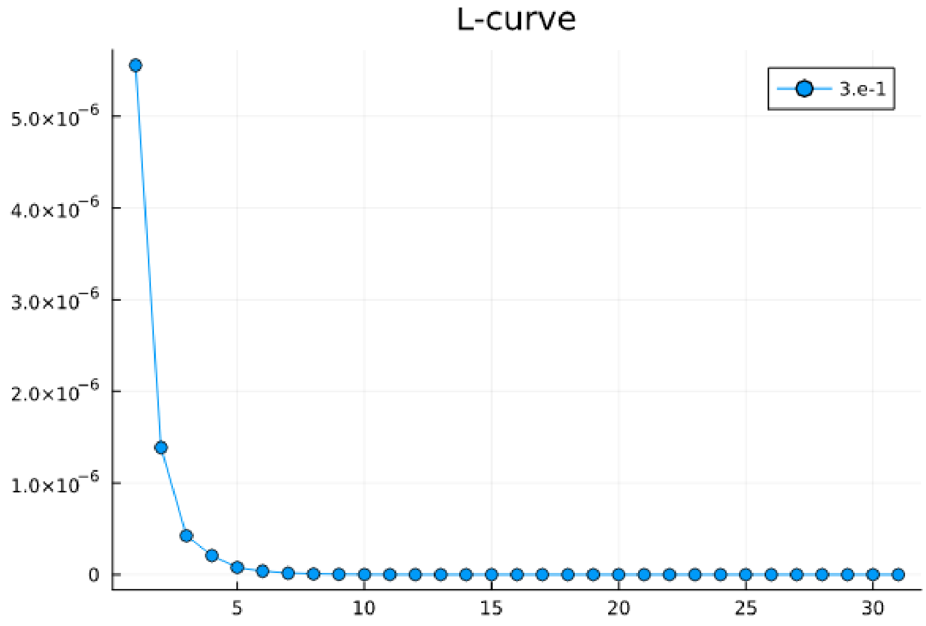

Figure 4.1 Residual Norm Plot For 3e-1

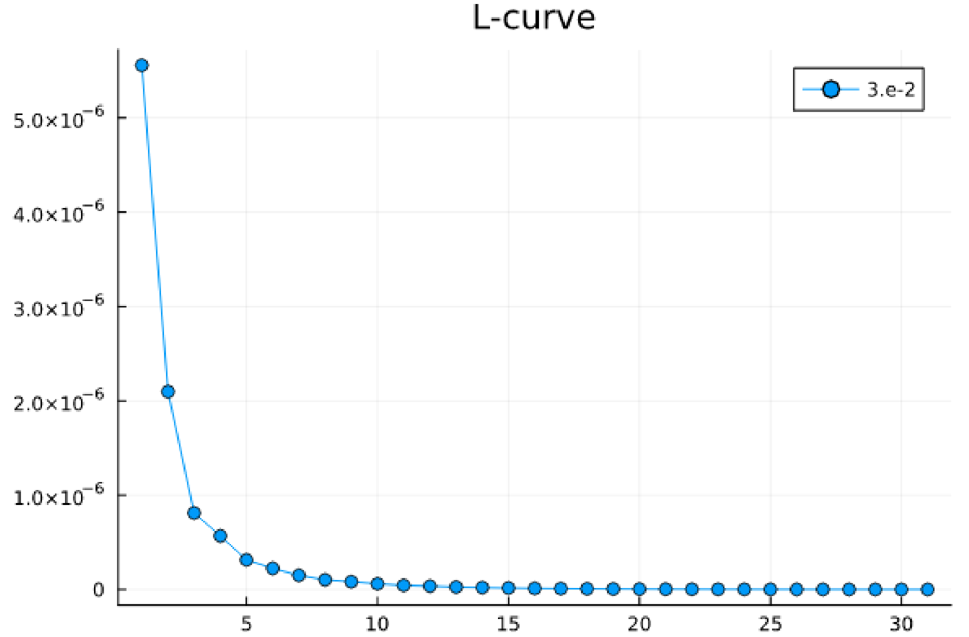

Figure 4.2 Residual Norm Plot For 3e-2

The plot in Figure 4.3 shows the logarithm of the residual norm (the error between the observed and predicted data) versus the logarithm of the regularization parameter λ for the in vivo data. The plot shows how different orders of magnitude of λ affect the data fit and solution smoothness.

The plot indicates that the logrithm (residual norm) increases as log(λ) increases from -4 to -0.5, which implies that smaller orders of magnitude of λ result in better data fit and more accurate solutions. However, the plot also shows that the slope of the curve decreases as log(λ) increases further, implying a diminishing return in data fit and accuracy for too large orders of magnitude of λ.

The plot also suggests that there is an optimal order of magnitude of λ that minimizes the log(residual norm) while avoiding overfitting or underfitting. The optimal order of magnitude of λ is usually located at the corner of the L-curve plot, corresponding to a good balance between data fit and solution smoothness. For this problem, λ's optimal order of magnitude seems to be around -3, as it provides the lowest log(residual norm) among the tested values.

Therefore, based on the plot, we can conclude that Tikhonov regularization with the CGNR method can effectively solve ill-conditioned linear systems of equations with a suitable order of magnitude of λ. The optimal order of magnitude of λ can be determined using the L-curve criterion or minimizing the log(residual norm).

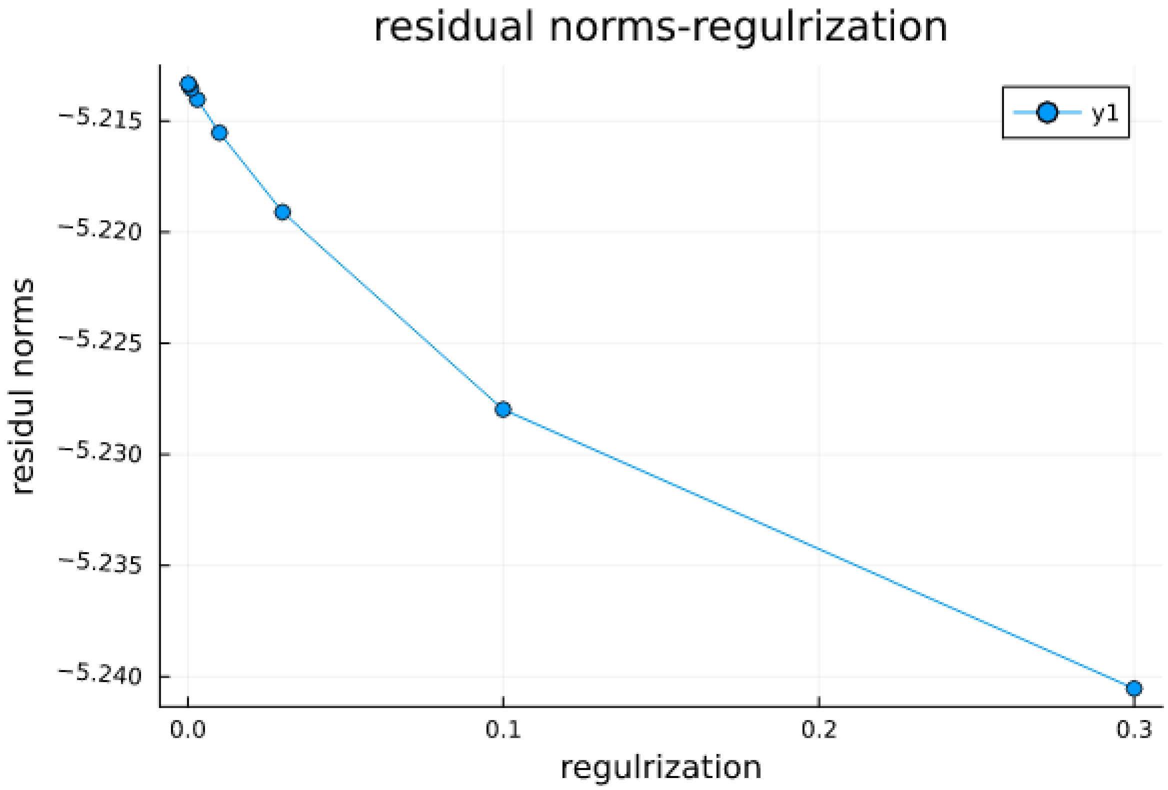

Figure 4.3 Residual Norm vs. Different Regularization values

The convergence plot for the 3D phantom data shows the residual norm versus the number of iterations for λ = 1e-2. The plot indicates that the residual norm decreases rapidly in the first few iterations and reaches a minimum value after 6 iterations. This suggests that the solution has converged to a desired accuracy in a relatively short time. The plot also shows that the convergence curve is smooth and stable, which implies that the CGNR method with Tikhonov regularization is robust and reliable.

The fast convergence for the 3D phantom data can be explained by the fact that this data set has no BO inhomogeneity, a source of noise and distortion in MRI reconstruction. Therefore, the data fit and solution smoothness are easier to achieve for this data set than for the in vivo data set, which has BO inhomogeneity. This also implies that λ = 1e-2 is a suitable value of regularization parameter for this data set, as it provides a good balance between data fit and solution smoothness.

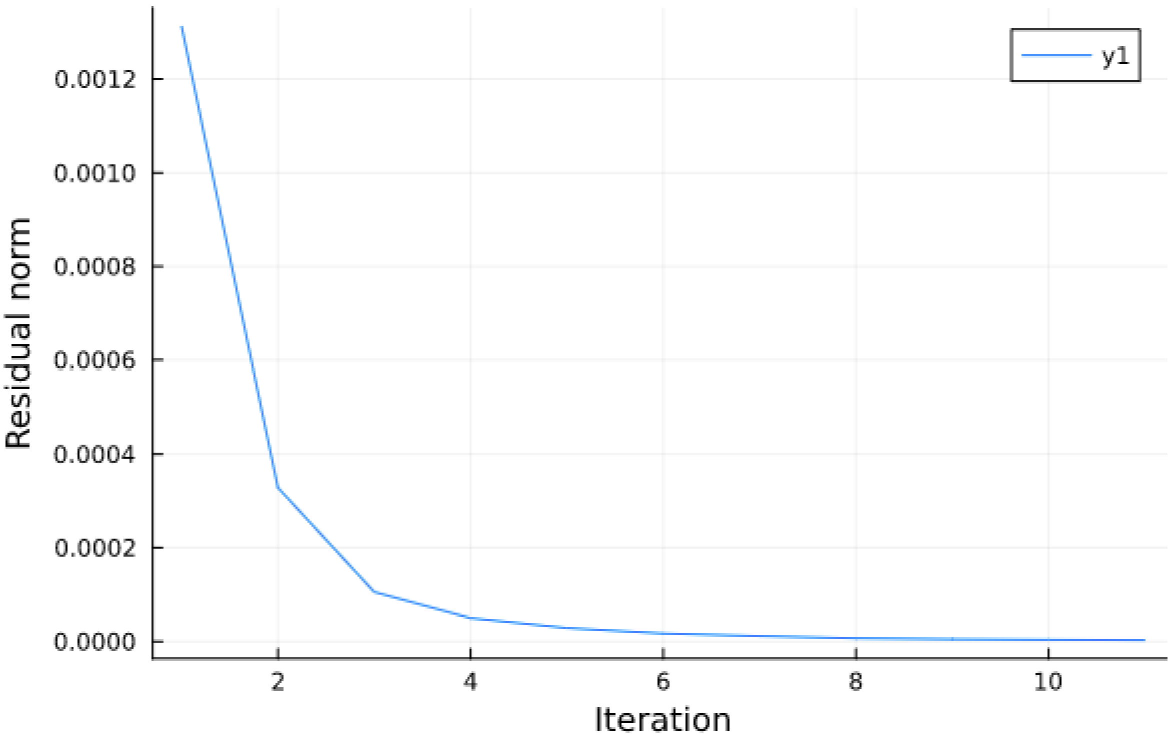

Figure 4.4 Residual Norm for 1e-2

For both data sets, the L-curve has a clear corner point, indicating an optimal λ value. For the 3D phantom dataset, the optimal λ is around 0.01. For the 3D human head dataset, the optimal λ is around 0.1.

For both data sets, smaller values of λ result in lower residual norms but require more iterations to converge. Larger values of λ result in higher residual norms but converge faster.

For both data sets, the convergence curves are smooth and stable, which suggests that the CGNR method with Tikhonov regularization is robust and reliable.

4.2 ADMM METHOD

The ADMM algorithm solves convex optimization problems that involve splitting the variables into two or more blocks and updating them alternately using proximal operators. The algorithm has a parameter ρ that controls the penalty for the constraint violation and affects the convergence rate and stability of the algorithm.

To investigate the effect of different values of ρ on the ADMM algorithm, we can run the algorithm with ρ = [1e-6,1e-2, 1.e-3, 1e2, 1.e6] and compare the results. We use the input of the 3D phantom data set with no BO inhomogeneity.

The results are shown in the following figures 4.5. 4.6 & 4.7:

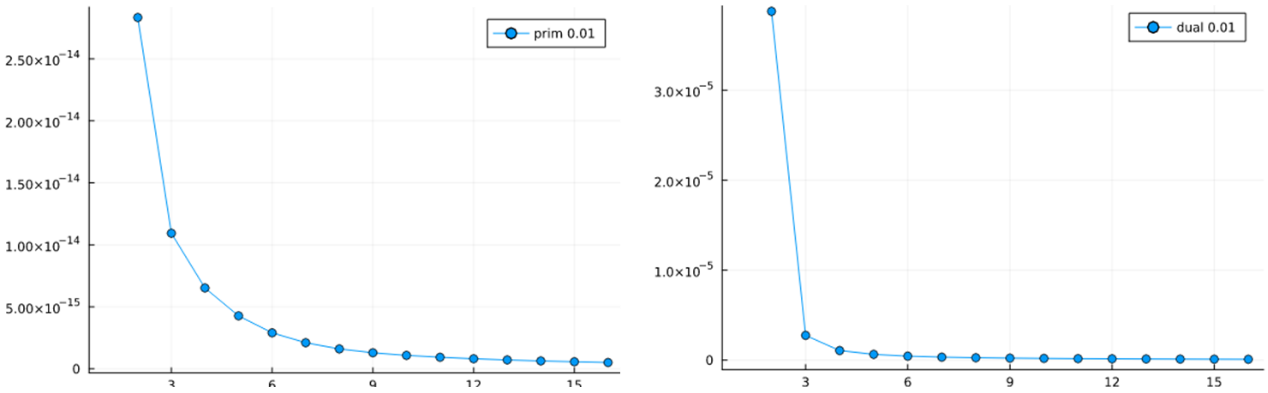

Figure 4.5 L-curve of primal and dual residual vs. iterations for ρ = 0.01

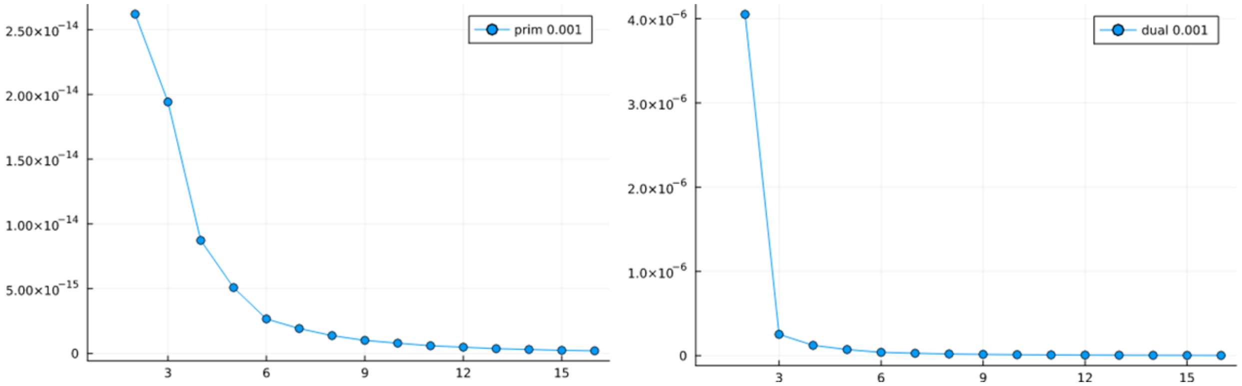

Figure 4.6 L-curve of primal and dual residual vs iterations for ρ = 0.001

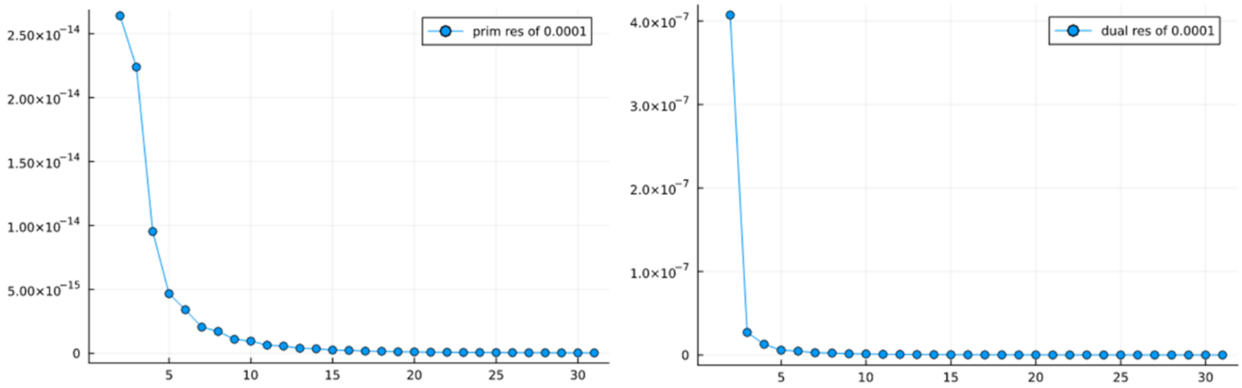

Figure 4.7 L-curve of primal and dual residual vs. iterations for ρ = 0.0001

The L-curve plots show how different values of ρ affect the convergence rate and stability of the ADMM algorithm. The plots show the primal residual (the error between the two blocks) and the dual residual (the error between the current and previous iterates) versus the number of iterations. The smaller the residuals, the more accurate and stable the solution.

The plots indicate that smaller values of ρ result in lower primal residuals but higher dual residuals. This implies that smaller values of ρ improve the data fit and solution smoothness but reduce the convergence speed and stability while increasing the number of iterations. Larger values of ρ result in higher primal residuals but lower dual residuals. This implies that larger values of ρ increase the convergence speed and stability but worsen the data fit and solution smoothness.

The plots also suggest an optimal range of ρ values that minimize primal and dual residuals while avoiding overfitting or underfitting. The optimal range of ρ values is usually located at the corner of the L-curve plot, where there is a good balance between data fit and solution smoothness, convergence speed, and stability. For this problem, the optimal range of ρ values seems to be around 0.001 to 0.01, as they provide the lowest residuals among the tested values.

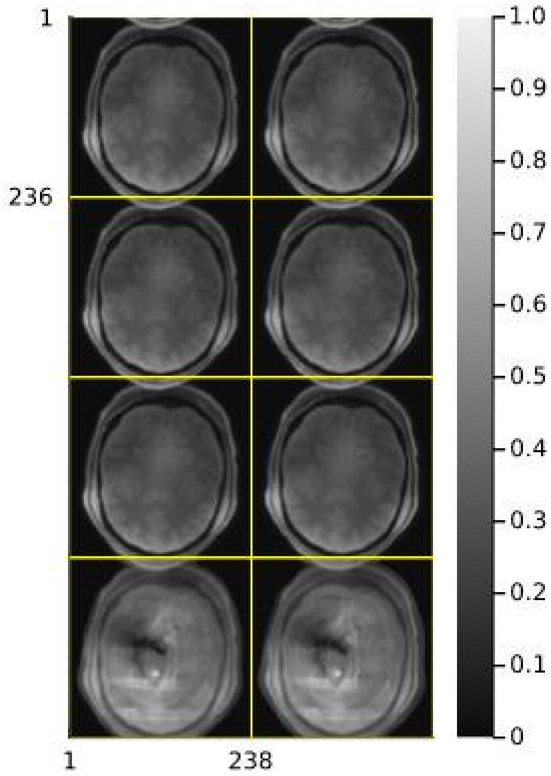

Figure 4.8 Two slices of reconstructed phantom for different ρ values top to bottom 1e-6, 1e-3, 1e-2, 1e3.

The images in the Figure 4.8 indicate that smaller values of ρ result in more accurate and detailed reconstructed images but also more noisy and distorted images. This implies that smaller values of ρ preserve more information from the original image and amplify more noise from the noisy image. Larger values of ρ result in less accurate and detailed reconstructed images and less noisy and distorted images. This implies that larger values of ρ filter out more noise from the noisy image but also lose more information from the original image.

The images also suggest that there is an optimal range of ρ values that produce high-quality and accurate reconstructed images while avoiding overfitting or underfitting. The optimal range of ρ values is usually consistent with the optimal range determined by the L-curve criterion. For this problem, the optimal range of ρ values seems to be around 0.001 to 0.01, as they produce clear and sharp reconstructed images.

Therefore, based on these results, we can conclude that different values of ρ significantly affect the performance and quality of the ADMM algorithm with Tikhonov regularization with the CGNR method for MRI reconstruction. The optimal value of ρ can be determined by using the L-curve criterion or by comparing the reconstructed images.

The difference images in Figure 4.9 number show the absolute value of the pixel-wise subtraction between the original image and the reconstructed images for different values of ρ. The various images reflect the error and noise level in the reconstructed images.

The difference images indicate that smaller values of ρ result in darker and smoother difference images but also more visible and irregular artifacts. This implies that smaller values of ρ produce more accurate and detailed reconstructed images that are close to the original image but also more noisy and distorted images that deviate from the original image in some regions. Larger values of ρ result in brighter and rougher difference images but also less noticeable and regular artifacts. This implies that larger values of ρ produce less accurate and detailed reconstructed images that are far from the original image but also less noisy and distorted images that are consistent with the original image in most regions.

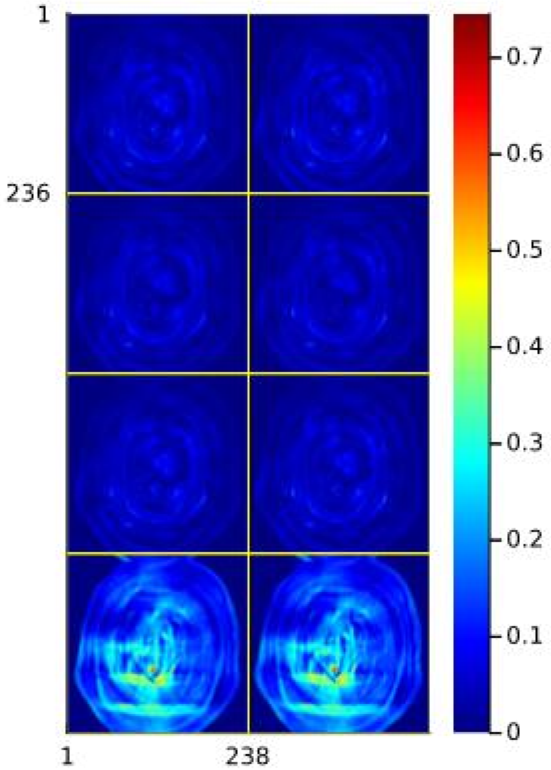

Figure 4.9 Difference images of reconstructed phantom for different ρ values top to bottom 1e-6, 1e-3, 1e-2, 1e3.

The difference images also suggest an optimal range of ρ values that produce optimal difference images, which are dark, smooth, and have minimal artifacts. The optimal range of ρ values is usually consistent with the optimal range determined by the L-curve criterion. For this problem, the optimal range of ρ values seems to be around 0.001 to 0.01, as they produce optimal difference images.

Therefore, based on these results, we can conclude that different ρ values significantly affect the performance and quality of the ADMM algorithm with Tikhonov regularization with the CGNR method for MRI reconstruction. The optimal value of ρ can be determined using the L-curve criterion or by comparing the different images.

The structural similarity index (SSIM) is a metric that compares the similarity between two images based on their luminance, contrast, and structure. The SSIM ranges from -1 to 1, where 1 means identical images and -1 means opposite images 1. The SSIM can be calculated using the JuliaImages package, which provides a collection of packages for image processing and machine vision in Julia 2.

The SSIM is better than the mean squared error (MSE), another metric that measures the difference between two images based on pixel values. The MSE is simple to calculate, but it may not reflect the perceived similarity of images, especially when they have different textures or noise levels. The SSIM considers texture, assigning a higher score to images that may appear similar 1.

The MSE is the average of the squared differences between the corresponding pixels of two images. The MSE can be calculated using the MSE function defined in ImageDistances. The MSE ranges from 0 to infinity, where 0 means identical images and infinity means opposite images.

The SSIM is a weighted combination of three terms: luminance (L), contrast ©, and structure (S). The luminance term measures the similarity of the average pixel values of two images. The contrasting term measures the similarity of the two images' standard deviations of pixel values. The structure term measures the similarity of the normalized covariances of pixel values of two images. The SSIM can be calculated using the assess_ssim function defined in the ImageQualityIndexes package. The SSIM also has a parameter ρ that controls the penalty for the constraint violation and affects the convergence rate and stability of the algorithm.

Table 4.2 indicates that the real part of SSIM is similar for ρ values of 1e-6, 1e-2, and 1e-3, which implies that these ρ values produce high-quality and accurate reconstructed images close to the original image in terms of luminance and contrast. However, the real part of SSIM is much lower for ρ value of 1e-3, which implies that this value of ρ produces a low-quality and inaccurate reconstructed image far from the original image in terms of luminance and contrast.

Table 4.2 SSIM for different values of ADMM penalty parameter

Method	**ρ**	**SSIM**
ADMM	1e-6	0.897 - 6.11e-6i
ADMM	1e-2	0.897 + 9.5e-5i
ADMM	1e-3	0.897 - 0.067i
ADMM	1e2	0.540 - 0.064i
CGNR	N/A	0.867 - 0.077i

Table 4.2 also shows that the imaginary part of SSIM is small for ρ values of 1e-6 and 1e-2, which implies that these values of ρ produce reconstructed images that are similar to the original image in terms of structure and orientation. However, the imaginary part of SSIM is larger for ρ values of 1e-3 and 1e2, which implies that these values of ρ produce reconstructed images that are different from the original image in terms of structure and orientation.

Table 4.2 also shows that the complex value of SSIM for CGNR reconstructed image with L2 regularization parameter 3e-2 is slightly lower than the complex values of SSIM for ADMM reconstructed images with optimal ρ values, which implies that the CGNR method with L2 regularization produces a slightly lower-quality and less accurate reconstructed image than ADMM method with optimal ρ values.

The images show how different values of ρ affect the quality and accuracy of the reconstructed images for two slices of phantom data set. The images show the original image, the noisy image, and the reconstructed image for each value of ρ.

The difference image between the image reconstructed by CGNR and the image reconstructed by ADMM shows the absolute value of the pixel-wise subtraction between the two images. The different images reflect the error and information loss in the reconstructed images.

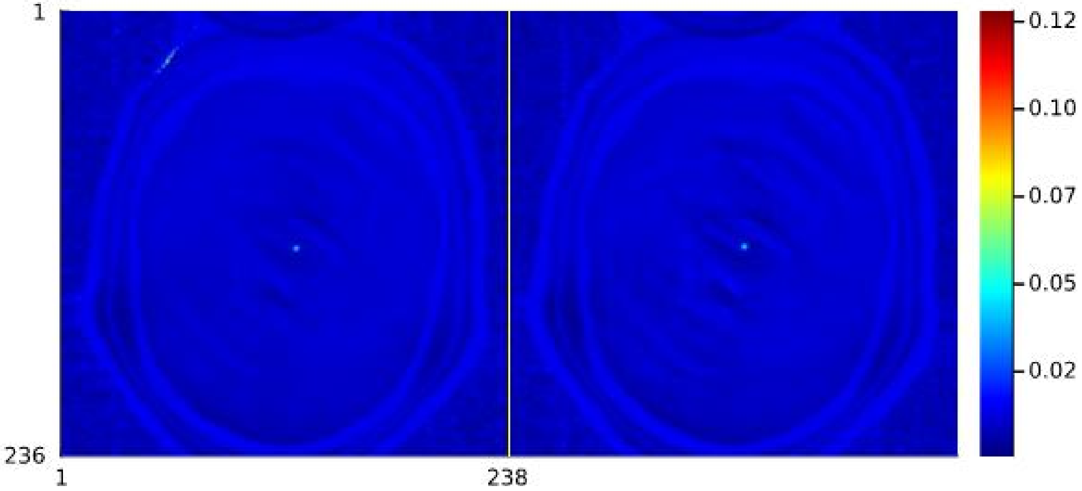

Figure 4.10 Difference image of CGNR Reconstructed phantom & ADMM reconstructed phantom

The difference image indicates that the image reconstructed by CGNR has more bright and rough regions than the image reconstructed by ADMM, which implies that the image reconstructed by CGNR has more error and information loss than the image reconstructed by ADMM. This is because the CGNR method with L2 regularization produces a less accurate and detailed reconstructed image than the ADMM method with optimal ρ values.

The difference image also suggests that the information loss in the image reconstructed by CGNR is mainly due to the smoothing effect of L2 regularization, which reduces the contrast and sharpness of the image. The smoothing effect also leads to a loss of texture and edge information, which are important for image quality and perception.

Therefore, based on the different images, we can conclude that the ADMM method with optimal ρ values produces a higher-quality and more accurate reconstructed image than the CGNR method with L2 regularization for MRI reconstruction. The different image also demonstrates the advantage of the ADMM method over the CGNR method in preserving more information from the original image.

4.3 G-FACTOR

The g-factor is an important metric for evaluating the quality of MRI images. It represents the degree of signal-to-noise amplification or reduction caused by parallel imaging techniques commonly used in 3D spiral imaging to reduce scan time. Multiple receiver coils acquire data simultaneously in parallel imaging, allowing faster imaging times. However, this technique can lead to an increase in noise and image artifacts. The g-factor is calculated as the ratio of the noise in the parallel imaging reconstruction to the noise in the fully sampled reconstruction and is used to quantify the reduction in image quality due to parallel imaging.

In 3D spiral imaging, the g-factor is particularly important because it can significantly impact image quality. Since 3D spiral imaging requires a long scan time, parallel imaging often reduces scan time and increases patient comfort. However, this can lead to a reduction in signal-to-noise ratio and image quality. By calculating the g-factor, researchers can evaluate the impact of parallel imaging on image quality and optimize imaging parameters to improve image quality.

Parallel imaging techniques are widely used in magnetic resonance imaging (MRI) to accelerate data acquisition and reduce scan time. However, parallel imaging also introduces noise amplification and aliasing artifacts, degrading signal-to-noise ratio (SNR), and image quality. The g-factor is commonly used as a measure of the SNR penalty due to parallel imaging to quantify the noise amplification and aliasing artifacts. The g-factor depends on various factors, such as the coil array, the reduction factor, the trajectory design, and the reconstruction method.

The main objective of this chapter is to evaluate and compare the g-factor for different types of spiral trajectories using a comprehensive quantification method. The complete quantification method is based on the work of Robson et al. (2008), who proposed a general framework for measuring the SNR and g-factor for image-based and k-space-based parallel imaging reconstructions. The method can be applied to any trajectory design and any coil array configuration, and it accounts for the noise correlation between coils and the reconstruction kernel. The method also provides a way to compare the g-factor for different trajectories and reconstructions using a common reference.

G-factor is calculated as:

$$g = \frac{\mathrm{SNR}_{\mathrm{optimal,unaccelerated}}}{\mathrm{SNR}_{\mathrm{accelerated}} \cdot \sqrt{R}} = \frac{\mathrm{SD}_{\mathrm{accelerated}}}{\mathrm{SD}_{\mathrm{optimal,unaccelerated}} \cdot \sqrt{R}}$$

There are different methods to estimate the g-factor, such as analytical, multiple replicas, and pseudo replica methods. Analytical methods require explicit knowledge of the reconstruction matrix and do not apply to all reconstruction algorithms. Multiple replica methods require repeated acquisitions of k-space data with different noise realizations and are time-consuming and impractical. Pseudo-replica methods are based on adding artificial noise to a single k-space acquisition and are fast, simple, and accurate.

In this work, the method for comprehensive quantification of SNR and g-factor for image-based and k-space-based parallel imaging reconstructions has been used, as proposed by Robson et al. (2008). This work explains how the method is applied to different spiral trajectories, such as variable-density spirals and stack-of-spirals.

In this work, the g-factor map is calculated by implementing the pseudo replica method in Julia. The Image reconstructions are performed by using the MRIReco.jl package. The MRIReco.jl package allows the user to generate and reconstruct the coil, reference, and under sampled images using different types of spiral trajectories and parallel imaging techniques.

4.3.1 PSEUDO REPLICA METHOD FOR FINDING G-FACTOR MAPS

The Pseudo replica method is a statistical technique used to estimate the variability of the g-factor in magnetic resonance imaging (MRI) data.[13] The g-factor measures the noise amplification caused by parallel imaging techniques used in MRI. The Pseudo replica method generates multiple noise realizations of the k-space data by adding random noise to the acquired data. The noise should have the same statistical characteristics as the original data.

The pseudo replica method performed a g-factor analysis for image variability. The pseudo-replica method consisted of the following steps:

1. MRI data were acquired using parallel imaging techniques with a variable density stack of spirals (VDSS) with an acceleration factor of 3.
2. 45 pseudo replicas of the k-space data were generated by adding random noise correlated with the noise covariance matrix obtained from the 32 channel coils of the scanner.
3. The noise was added to the k-space of the original image data, and the missing k-space lines were zero-filled.
4. The images were reconstructed using the SENSE reconstruction method with regularization parameters optimized for each coil sensitivity map.
5. Steps 2-4 were repeated for each pseudo replica.
6. The standard deviation maps of the noise-only replicas and the noisy image replicas across the 45 iterations were computed.
7. The g-factor maps were calculated by dividing the standard deviation map of the noise-only replicas by the standard deviation map of the noisy image replicas.

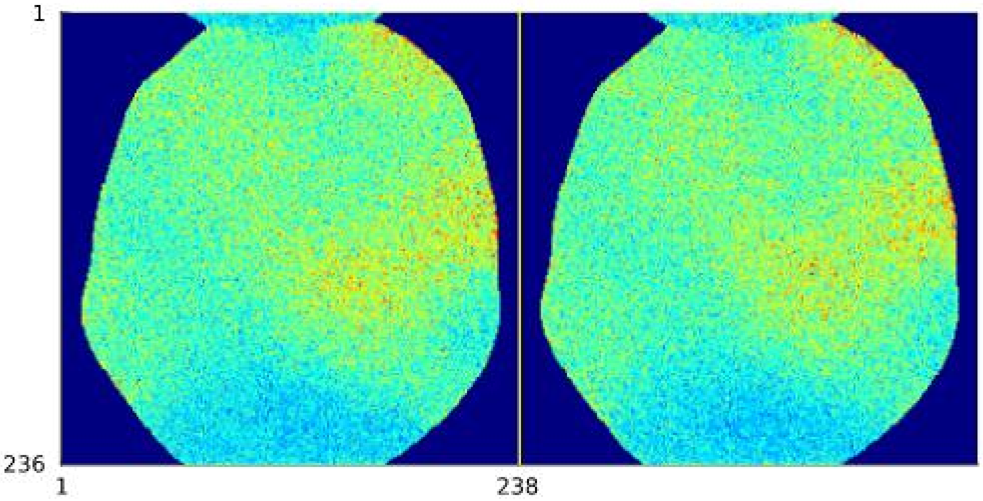

Figure 4.11 The SD map of zero-filled k-space noise replicas

The standard deviation map of noise replicas for two slices of 3D phantom head with zero filled k-space is showed in Figure 4.11. The g-factor maps of the 3D simulated phantom data are shown in Figure 4.12. The standard deviation maps indicate the noise level in each image pixel, while the g-factor maps indicate the noise amplification due to parallel imaging. The results show that the VDSS with R=3 has a lower noise level and g-factor than the SS with R=3, indicating that the VDSS technique can reduce noise amplification and improve image quality. The results also show that the pseudo-replica method can provide reliable estimates of the g-factor and the image variability for different parallel imaging techniques.

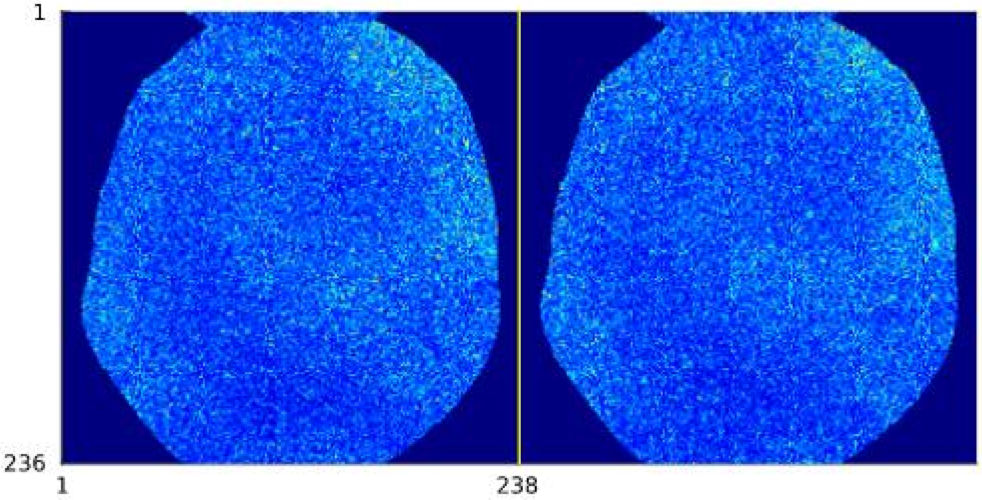

Figure 4.12 Standard deviation of Stack of spiral simulated replicas of phantom

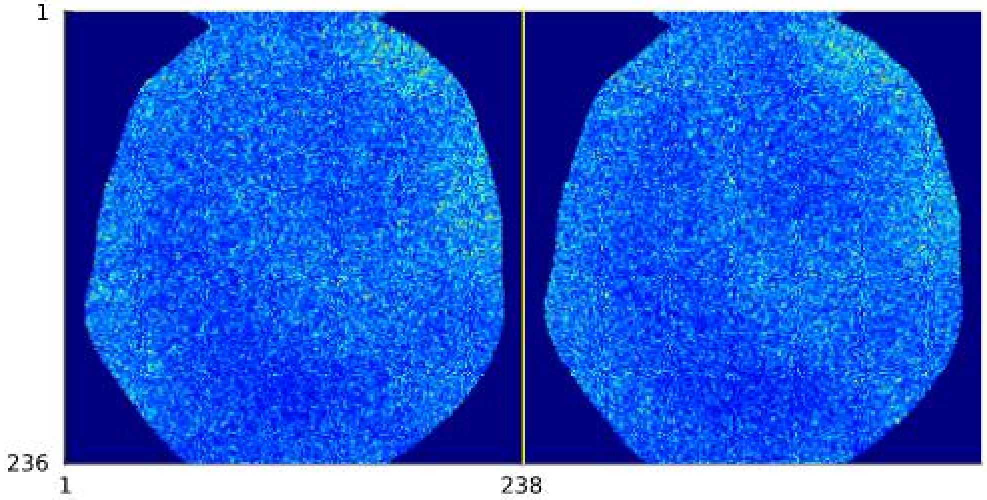

Figure 4.13 Standard deviation of variable density Stack of spiral simulated replicas of phantom

Standard deviation maps and g-factor maps of the 3D simulated phantom data for VDSS with R=3 and SOSP with R=3. The pseudo-replica method was used to generate 45 noise realizations for each technique.

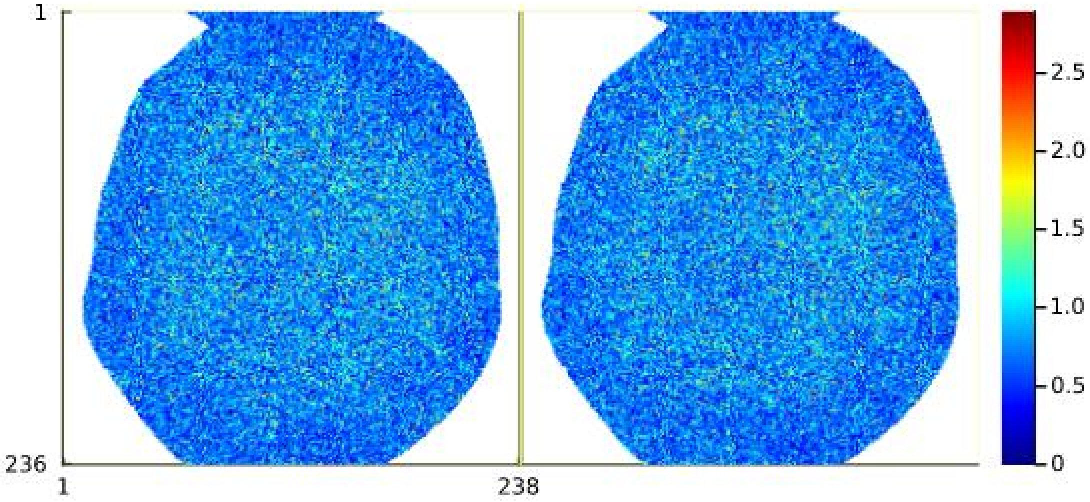

Figure 4.14 G-Factor map of Stack of spiral simulated phantom

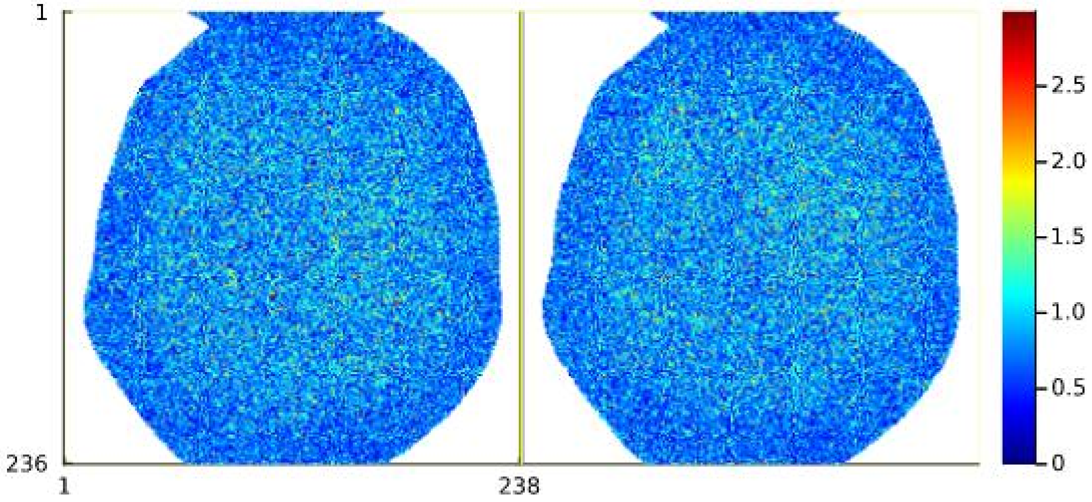

Figure 4.15 G-Factor map of variable density stack of spiral simulated phantom

5 CHAPTER: DISCUSSION AND CONCLUSION

This thesis work has investigated and performed experiments for different reconstruction methods for 3D MRI data acquired using parallel imaging techniques. The main reconstruction methods studied were conjugate gradient normal residual (CGNR) and alternating direction method of multipliers (ADMM). The performance of these methods was evaluated for different parameters such as regularization, acceleration factor, and coil sensitivity maps. The convergence curves of the residual norms in CGNR and the primal and dual residuals in ADMM were plotted and analyzed. The thesis also implemented the pseudo replica method for 3D image reconstruction to test the image variability for different sampling trajectories, such as a stack of spirals and variable density stack of spirals. The pseudo replica method generated multiple noise realizations of the k-space data and reconstructed the images using the SENSE method. The reconstructed images' standard deviation and g-factor maps were computed and compared for different sampling trajectories. The results showed that the VDSS technique could achieve better image quality and lower noise amplification than the Stack of Spirals. The results also showed that the CGNR and ADMM methods could provide accurate and robust reconstruction of 3D MRI data with different parameters.

The main contributions of this thesis work are:

- The development and implementation of CGNR and ADMM methods for 3D MRI reconstruction with parallel imaging techniques.
- Comparing and analysis of the convergence behavior and reconstruction performance of CGNR and ADMM methods for different parameters.
- Implementing and applying the pseudo replica method for 3D image reconstruction to test the image variability for different sampling trajectories.
- The demonstration of the advantages of the VDSP technique over SOSP

The main limitations of this thesis work are:

- Using simulated phantom data instead of real patient data may not reflect the true complexity and variability of human anatomy and physiology.
- The use of the SENSE reconstruction method as a baseline may not be optimal for highly accelerated parallel imaging techniques.

The main directions for future work are:

- To apply the proposed reconstruction methods to real patient data acquired with different parallel imaging techniques and compare them with clinical standards.
- To explore other regularization techniques such as total variation, low-rank, or sparsity-promoting priors to improve the reconstruction quality and stability.

- To investigate other deep learning-based reconstruction methods such as U-net, MoDL, or PnP-ADMM and compare them with the proposed methods in speed, accuracy, and robustness.
- To extend the pseudo replica method to other types of MRI data such as diffusion-weighted imaging, functional MRI, or spectroscopic imaging and assess their variability and reliability.

6 BIBLIOGRAPHY

[1] F. Bloch,W.W. Hansen, and M. Packard. Nuclear induction. Phys. Rev., 69(3-4):127, Feb 1946.

[2] Pruessmann KP, Weiger M, Scheidegger MB, Boesiger P. SENSE: sensitivity encoding for fast MRI. Magn Reson Med 1999; 42: 952–962.

[3] Griswold MA, Jakob PM, Heidemann RM, Nittka M, Jellus V, Wang J, Kiefer B, Haase A. Generalized Autocalibrating Partially Parallel Acquisitions (GRAPPA). Magn Reson Med 2002; 47: 1202–1210.

[4] MacRobbie, Donald W., et al. MRI from Picture to Proton. Cambridge University Press, 2017.

[5] Nobel Web AB. The nobel prize in physics1952, 2008. http://nobelprize.org/nobel_prizes/physics/laureates/1952/.

[4] Bezanson J, Edelman A, Karpinski S, Shah VB. Julia: A fresh approach to numerical computing. SIAM Rev. 2017; 59: 65- 98.

[5] Hansen MS, Sørensen TS. Gadgetron: an open source framework for medical image reconstruction. Magn Reson Med. 2013; 69: 1768- 1776.

[6] Uecker M, Ong F, Tamir JI, et al. Berkeley advanced reconstruction toolbox. Proc Int Soc Mag Reson Med. 2015; 23: 2486.

[7] Ong F, Lustig M. SigPy: a python package for high performance iterative reconstruction. Proc Int Soc Mag Reson Med. 2019; 27: 4819.

[8] Eggers H, Knopp T, Potts D. Field inhomogeneity correction based on gridding reconstruction for magnetic resonance imaging. IEEE Trans Med Imaging. 2007; 26: 374- 384.

[9] Knopp, T, Grosser, M. MRIReco.jl: An MRI reconstruction framework written in Julia. Magn Reson Med. 2021; 86: 1633– 1646. https://doi.org/10.1002/mrm.28792

[10] Henkelman RM. Measurement of signal intensities in the presence of noise in MR images [Published erratum in Med Phys 1986;13:544]. Med Phys 1985; 12: 232–233.

[11] Constantinides CD, Atalar E, McVeigh ER. Signal-to-noise measurements in magnitude images from NMR phased arrays. [Published erratum in: Magn Reson Med. 2004 Jul;52:219]. Magn Reson Med 1997; 38: 852–857.

[12] Sijbers J, Den Dekker AJ, Van Audekerke J, Veρye M, Van Dyck D. Estimation of the noise in magnitude MR images. Magn Reson Imaging 1998; 16: 87–90.

[13] Robson, P.M., Grant, A.K., Madhuranthakam, A.J., Lattanzi, R., Sodickson, D.K. and McKenzie, C.A. (2008), Comprehensive quantification of signal-to-noise ratio and g-factor for image-based and k-space-based parallel imaging reconstructions. Magn. Reson. Med., 60: 895-907. https://doi.org/10.1002/mrm.21728

[14] D. C. Noll, "Reconstruction Techniques for Magnetic Resonance Imaging," Ph.D. dissertation, Stanford Univ., Stanford, CA, 1991

[15] L.-C. Man, J. M. Pauly, and A. Macovski, "Multifrequency interpolation for fast off-resonance correction," Mag. Res. Med., vol. 37, pp. 785–792, 1997

[16] J. A. Fessler, Sangwoo Lee, V. T. Olafsson, H. R. Shi and D. C. Noll, "Toeplitz-based iterative image reconstruction for MRI with correction for magnetic field inhomogeneity," in IEEE Transactions on Signal Processing, vol. 53, no. 9, pp. 3393-3402, Sept. 2005, doi: 10.1109/TSP.2005.853152.

[17] Hestenes MR, Stiefel E. Methods of conjugate gradients for solving linear systems. J Res Nat Bureau Standards. 1952; 49.

[18] Parikh N, Boyd S, et al. Proximal algorithms. Foundations Trends® Optim. 2014; 1: 127-239.

[19] Deshmane, Anagha, et al. "Parallel MR Imaging." Journal of Magnetic Resonance Imaging, vol. 36, no. 1, 2012, pp. 55–72., doi:10.1002/jmri.23639